


## Nanofiber-Induced Losses Inside an Optical Cavity

Bernd Welker<sup>1</sup>,<sup>✉</sup> Thorsten Österle,<sup>1</sup> Sebastian Slama<sup>1,\*</sup>, Thomas Hoinkes,<sup>2</sup> and Arno Rauschenbeutel<sup>2</sup>

<sup>1</sup>*Center for Quantum Science and Physikalisches Institut, Eberhard-Karls Universität Tübingen, Auf der Morgenstelle 14, 72076 Tübingen, Germany*

<sup>2</sup>*Department of Physics, Humboldt-Universität zu Berlin, 10099 Berlin, Germany*

 (Received 12 July 2021; revised 28 October 2021; accepted 24 November 2021; published 8 December 2021)

Optical high-finesse cavities are a well-known means to enhance light-matter interactions. Despite much progress in the realization of strongly coupled light-matter systems, the controlled positioning of single solid emitters in cavity modes remains a challenge. We pursue the idea of using nanofibers with subwavelength diameter as a substrate for such emitters. This paper addresses the question of how strongly optical nanofibers influence the cavity modes. We analyze the influence of the fiber position for various fiber diameters on the finesse of the cavity and on the shape of the modes.

DOI: [10.1103/PhysRevApplied.16.064021](https://doi.org/10.1103/PhysRevApplied.16.064021)

### I. INTRODUCTION

Strong coupling between light and matter is a hallmark of light-matter interactions and has been demonstrated in various systems using optical cavities[1]. It is reached when the coupling constant  $g_0 \propto 1/\sqrt{V_m}$  with cavity mode volume  $V_m$  is larger than the excited-state linewidth  $\gamma$  of the emitter and the cavity linewidth  $\kappa$  (the light field decay rate). Two complementary approaches exist for the setup of these cavities in order to enhance the coupling. One approach minimizes  $V_m$  by building micro- and nanocavities, for instance with photonic crystal structures [2,3], micropillars [4], microdisks [5,6], arrays of nanovoids [7], and plasmonic nanostructures [8,9]. The reduction of mode volume is connected with a reduction of the cavity round-trip length  $l$ , which in turn increases the free spectral range  $\nu_{\text{FSR}} = c/l$  of the cavity and, correspondingly, the cavity full width at half maximum  $\nu_{\text{FWHM}} = \kappa/\pi = \nu_{\text{FSR}}/F$  for given cavity finesse  $F$ . The finesse in nanocavities is limited by the unavoidable optical loss due to the optical properties of the materials (in particular of metals) and due to imperfections in the fabrication process. Moreover, emitters cannot be easily inserted or exchanged in nanoscale cavities. The second approach focuses on maximizing the finesse of the cavity by using superpolished mirrors made of dielectric layers with low optical loss. The best cavities can reach a finesse of the order of  $F \sim 0.5 \times 10^6$  [10]. They are typically coupled with ultracold atoms that are trapped in optical or magnetic traps in vacuum and can be positioned relative to the cavity mode with high precision. This is more complicated for solid emitters, which are typically embedded in a dielectric substrate in the cavity [11] or are placed directly on one of the cavity

mirrors [12]. The existence of a substrate limits the finesse due to additional optical losses by reflection at the substrate boundaries. Following the trapping of cold atoms, impressive progress has been made on the levitation and motional cooling of nanoparticles using Paul traps [13,14] and optical tweezers [15]. However, this approach is not applicable for arbitrary particles and requires extensive use of optics and servo loops.

This paper investigates a substrate-based approach where the former plane substrate is replaced by an optical nanofiber. The latter are fabricated from standard step-index optical fibers in a heat-and-pull process, yielding a tapered optical fiber (TOF) with a subwavelength-diameter waist [16]. Optical emitters can be attached to these nanofibers, as demonstrated for nanocrystals [17–19], nitrogen-vacancy centers in diamond [20], and gold nanospheres [21]. Since the TOF allows one to efficiently couple light into and out of the nanofiber waist, it can serve not only as a substrate but also as a fiber-optical interface, which allows one to efficiently excite the emitter and to collect its fluorescence. Because of the subwavelength diameter, optical losses in the cavity due to the nanofiber are expected to be small. We analyze these losses by measuring the finesse of the cavity while nanofibers with various diameters are moved transversally through the mode. A similar setup has previously been used for measuring the optomechanical interaction between a nanowire and a cavity mode [22].

### II. EXPERIMENTAL SETUP

The experimental setup is schematically shown in Fig. 1. An optical cavity is formed by two spherical dielectric mirrors with radius of curvature  $R_c = 6$  cm and intensity transmission of  $T = 0.25\%$ . One of the mirrors is attached

\*sebastian.slama@uni-tuebingen.de

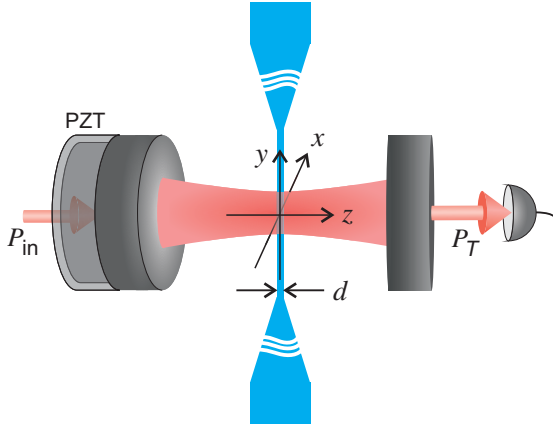


FIG. 1. (Not to scale.) A nanofiber with diameter  $d$  is moved in the  $x$  direction transversally through the mode of a cavity with free spectral range of  $\nu_{\text{FSR}} = 2.34$  GHz and finesse  $F_0 = 1240$  (value without fiber). One of the mirrors is attached to a PZT for scanning the cavity length. For fixed  $x$  position of the nanofiber the cavity linewidth  $\nu_{\text{FWHM}}$  is determined from the cavity transmission.

to a piezoelectric transducer (PZT). The free spectral range  $\nu_{\text{FSR}} = 2.34$  GHz of the cavity is calculated from the distance of the two mirrors of  $l/2 = 6.4$  cm. The beam waist ( $1/e$ -intensity radius) in the center of the cavity is  $w_0 = 86$   $\mu\text{m}$ . A laser field with power  $P_{\text{in}} = 3$  mW is coupled into the cavity through one of the mirrors. The laser field is generated by a free-running external cavity diode laser with wavelength  $\lambda = 780$  nm and 100-kHz laser linewidth. Sidebands are generated by modulating the laser current with frequency  $\nu_{\text{rf}} = 22.1184$  MHz in order to provide a frequency reference for the cavity spectrum. The spectrum is recorded by scanning the length of the cavity with the PZT, and monitoring the cavity transmission  $P_T$  on a photodiode. A typical scan over the  $\text{TEM}_{00}$  mode is shown in Fig. 2. The cavity linewidth is determined from a fit of the measured transmission. The distance between the two sidebands defines the frequency scale. However, they cannot be observed in the transmission signal at the same scale as the carrier. For that reason we simultaneously monitor a Pound-Drever-Hall signal in reflection from the cavity [23], from which we determine the frequency scale.

TOFs with waist diameters of  $d = 150, 300, 500,$  and  $1000$  nm are fabricated in a heat-and-pull process using a home-built computer-controlled fiber-pulling rig [24]. Each TOF is then fixed on a mechanical mount, which we attach to a nanopositioning stage (Attocube ECS3030), so that it can be moved with high precision in both the  $x$  and  $z$  directions.

### III. RESULTS

The finesse is analyzed as a function of the fiber position  $x$  transverse to the cavity mode. The result for the

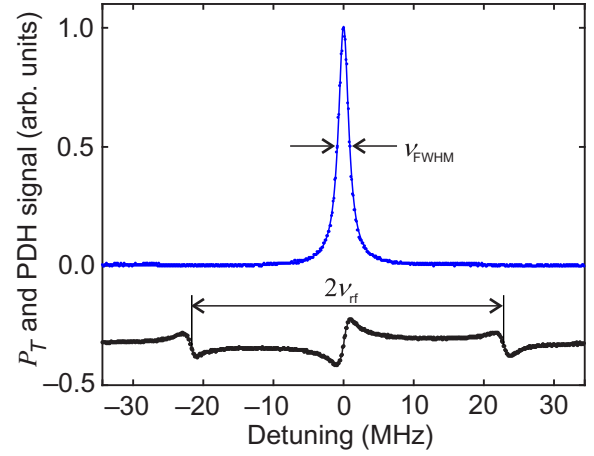


FIG. 2. The cavity length is scanned across the resonance of a  $\text{TEM}_{00}$  mode. The cavity full width at half maximum  $\nu_{\text{FWHM}}$  is determined from the measured cavity transmission  $P_T$  (blue data points). The frequency reference is given by the Pound-Drever-Hall signal (black data points).

300-nm-thick fiber is shown in Fig. 3. It is reduced from a value of  $F_0 = 1240$  without fiber to a minimum value of  $F = 650$  when the fiber is in the center of the mode. Only little reduction of finesse to  $F > 1000$  is measured for the thinnest nanofiber tested with a diameter of 150 nm. In contrast, no finesse variation can be detected when the fiber is displaced in the  $z$  direction along the cavity axis, where the mode function is given by the optical standing wave. In order to probe the field modulation of the standing wave the fiber must be orthogonal to the mode axis with an angle deviation of  $\alpha \lesssim \lambda/2(2w_0) = 0.23$  mrad. This is not the case in the present setup. The effective loss is given by an average over different positions along  $z$ . Independently of the tilt, an emitter on the nanofiber can always be placed in the antinode and on the axis of the cavity mode by shifting the nanofiber along the  $x$ ,  $y$ , and  $z$  directions. In fact, the tilt is even desirable because it reduces the cavity losses compared with the situation where the nanofiber is orthogonal to the cavity axis. In the latter case, placing the emitter in the antinode implies that the nanofiber fully lies in the antinodal plane. This leads to the highest possible loss. By comparison, for a tilted nanofiber, the loss is reduced by a factor of about 2 because the tilted fibers average over antinodes and nodes (where the loss is minimal) of the cavity field.

The fiber-induced optical loss in the cavity is simulated as light scattering of the incident mode field from a circular cylinder (the fiber) following Ref. [25]. The refractive index of the cylinder is homogeneous to a very good approximation, as the fiber core is approximately 20 times smaller than the fiber diameter, and its refractive index differs from that of the cladding by less than 1%. The mode is simulated as two counter-propagating plane waves with

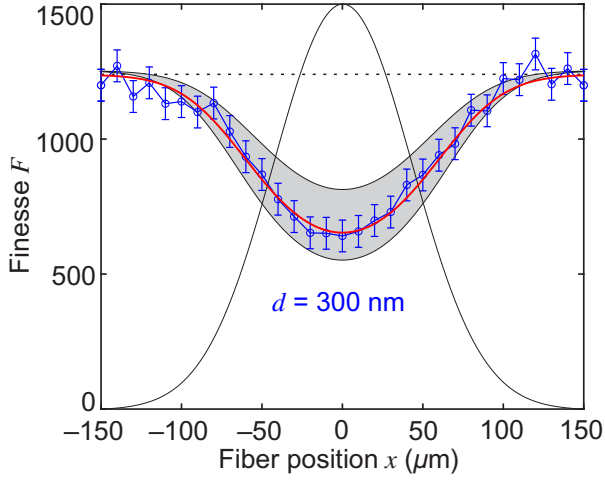


FIG. 3. Experimentally determined finesse of the cavity (blue data) for different fiber positions  $x$  of the  $d = 300$ -nm-thick fiber relative to the  $\text{TEM}_{00}$  mode (Gaussian lineshape). The dashed black line with a finesse of  $F_0 = 1240$  corresponds to the empty cavity with mirror intensity transmission  $T = 0.253\%$ . Error bars indicate the statistical variation of the determined finesse. Our model (red solid line) quantitatively agrees with the data. The gray shaded region indicates the accessible range by changing the polarization of the intracavity field.

perpendicular incidence onto the fiber:

$$u_{\text{inc}} = u_0 e^{-ikz + i\omega t} + u_0 e^{ikz + i\omega t + i\phi}, \quad (1)$$

where the phase  $\phi$  defines the position in the standing wave. Each incident wave generates a scattered wave of the form

$$u(r, \theta) = \sqrt{\frac{2}{\pi kr}} u_0 e^{-ikr + i\omega t - i3\pi/4} T_{s,p}(\theta), \quad (2)$$

valid in the far field ( $kr \gg d$ ), with distance  $r$  from the fiber and angle deviation  $\theta$  from the incident  $k$  vector, both given in the  $xz$  plane. The scattered field depends on the polarization ( $s$  or  $p$ ) of the incident light field relative to the fiber and is invariant in the  $y$  direction. The angle dependence is contained in the amplitude functions

$$T_s(\theta) = b_0 + 2 \sum_{n=1}^{\infty} b_n \cos(n\theta), \quad (3)$$

$$T_p(\theta) = a_0 + 2 \sum_{n=1}^{\infty} a_n \cos(n\theta), \quad (4)$$

where the coefficients are given by Bessel functions  $J_n(z)$  of first kind and second Hankel functions  $H_n(z)$  and their

derivatives  $J'_n(z)$  and  $H'_n(z)$  via

$$b_n = \frac{m J_n(y) J_n(x) - J_n(y) J'_n(x)}{m J'_n(y) H_n(x) - J_n(y) H'_n(x)}, \quad (5)$$

$$a_n = \frac{J'_n(y) J_n(x) - m J_n(y) J'_n(x)}{J'_n(y) H_n(x) - m J_n(y) H'_n(x)}. \quad (6)$$

In these equations,  $x = kd$  and  $y = mkd$ , and  $m$  denotes the refractive index of the fiber. The scattered total field is given by the superposition of the amplitude functions in opposite directions:

$$T_{s,p}^{\text{tot}}(\theta) = T_{s,p}(\theta) + e^{i\phi} T_{s,p}(\pi - \theta), \quad (7)$$

corresponding to the scattered fields from the two counter-propagating incident fields. The total power scattered by a fiber at position  $x$  is calculated via integration of the scattered intensity around and along the fiber:

$$P_{\text{scatt},s,p} = \int_0^{2\pi} r d\theta \int_{-\infty}^{+\infty} dy \left[ \frac{2}{\pi kr} \left| T_{s,p}^{\text{tot}}(\theta) \right|^2 I(x, y) \right], \quad (8)$$

which is proportional to the incident intensity  $I_0$  with Gaussian profile

$$I(x, y) = I_0 e^{-2(x^2 + y^2/w_0^2)}, \quad (9)$$

and thus to the light power

$$P_{\text{cav}} = \frac{1}{2} \pi w_0^2 I_0 \quad (10)$$

circulating in the cavity. The power loss per cavity round-trip caused by the fiber is given by

$$L_{s,p} = P_{\text{scatt},s,p} / P_{\text{cav}}. \quad (11)$$

This definition neglects scattering into resonant modes of the cavity not contributing to cavity loss, which is a valid approximation for the beam divergence of the cavity mode in our experiment. Moreover, scattering into guided modes of the nanofiber that could be caused by surface roughness or pollutants on the surface is negligible, as the nanofiber features a rms roughness at the nanometer scale. The finesse of the cavity is connected with the fiber loss via

$$F = \frac{\pi \sqrt{r_m}}{1 - r_m}, \quad (12)$$

with round-trip field reflectivity

$$r_m = \sqrt{1 - L - T_1 - T_2}, \quad (13)$$

and cavity mirror transmissions  $T_{1,2}$ . It depends periodically on the position  $z$  of the fiber along the optical

standing wave and on the light polarization. As the fiber in the experiment is slightly tilted with respect to the standing wave, we take the average of the finesse over one period. The results for the two polarizations (*s* and *p*) define the upper and lower bound of the finesse enclosing the gray shaded area in Fig. 3. Experimentally, we couple circularly polarized light into the cavity, giving rise to a circularly polarized standing wave inside the cavity. We describe the latter by an incoherent mixture of *s* and *p* polarization with mixing angle  $\beta = 45^\circ$ . The effective loss is thus given by

$$L = \cos(\beta)^2 L_p + \sin(\beta)^2 L_s. \quad (14)$$

We now investigate how the cavity loss depends on the fiber diameter. Results are shown in Fig. 4. The red circles are determined from the experimental data shown in Fig. 3 and equivalent data for the other fiber diameters. They correspond to the maximum loss when the fiber is in the center of the mode. The experimental uncertainty is within the circle diameter. We see that the loss is strongly reduced for fiber diameters well below the optical wavelength of 780 nm. The data are consistent with the theoretical calculation using the model explained above. It is notable that the loss is slightly larger when the light field is polarized parallel to the fiber. Moreover, small oscillations are observed in the simulation that can be attributed to optical resonances in the fiber. These resonances are beyond the scope of this work. Figure 4 also illustrates how the losses depend on the optical wavelength. Shorter wavelengths lead to more pronounced oscillations. Larger wavelengths lead to smaller losses, at least for small fiber diameters.

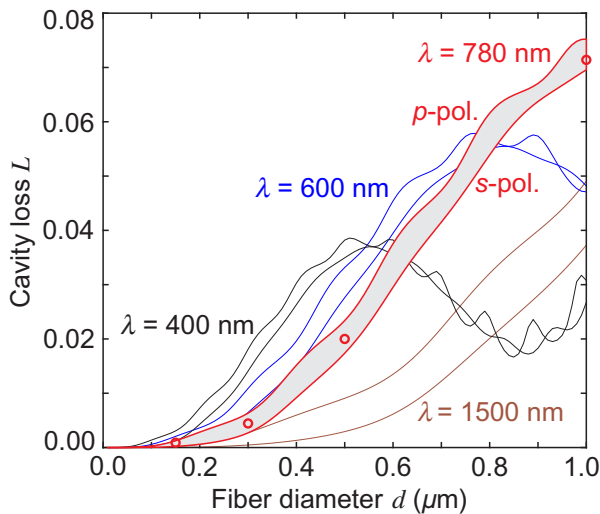


FIG. 4. Optical loss in the cavity caused by a dielectric fiber of diameter  $d$  in the center of the mode. Red circles are experimentally determined values, and solid lines are derived from the model for light polarization along (*p*) and perpendicular to (*s*) the fiber. For comparison, simulation results are presented for different optical wavelengths.

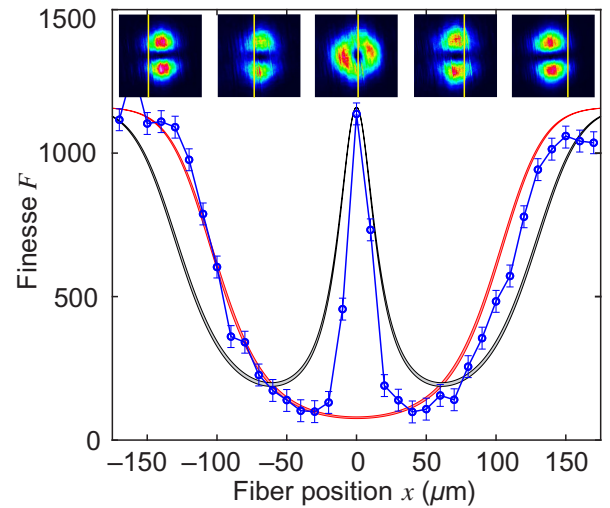


FIG. 5. The finesse in a  $TEM_{10}$  mode has a sharp maximum when the fiber is in the center of the mode. In this case, only the near-degenerate  $TEM_{01}$  mode is excited whose node line is parallel to the fiber axis. The fiber diameter is  $d = 1 \mu\text{m}$ . The mode shapes are detected by imaging the light beam transmitted through the cavity with a camera. The approximate position of the fiber (not to scale) is included in the images. The red and black lines correspond to the loss rates expected for a  $TEM_{00}$  mode and  $TEM_{01}$  mode, respectively.

In order to study the influence of the beam waist on the performance of the system, the scattering loss per cavity round-trip is calculated from (8)–(11) as

$$L_{s,p} = \frac{2}{\pi k w_0} \sqrt{\frac{2}{\pi}} \int_0^{2\pi} |T_{s,p}^{\text{tot}}(\theta)|^2 d\theta e^{-2x^2/w_0^2}, \quad (15)$$

i.e.,  $L \propto 1/w_0$ . It is also evident from (15) that the loss is proportional to the local intensity at the fiber position along the  $x$  direction, valid in the limit of  $d \ll w_0$ , as observed in Figs. 4 and 5. The corresponding finesse is calculated in the limit where the round-trip loss is dominated by scattering from the nanofiber, and not by the mirror transmission, i.e.,  $L \gg T_1, T_2$ . We further assume that the finesse is not too low, i.e.  $L \ll 1$ , and derive from (12) and (13) the proportionality  $F \propto w_0$ . A smaller beam waist will thus lead to a lower finesse. The actual figure of merit for light-matter interactions in terms of sensitivity is given by the cooperativity [12]

$$C \propto F \frac{\lambda^2}{w_0^2} \propto w_0 \frac{\lambda^2}{w_0^2} \propto \frac{1}{w_0}. \quad (16)$$

Small beam waists are thus favorable for strong light-matter interactions, also when taking into account the increased round-trip losses caused by the nanofiber.

The situation is more complicated for higher transverse TEM modes of the cavity, where near-degenerate modes

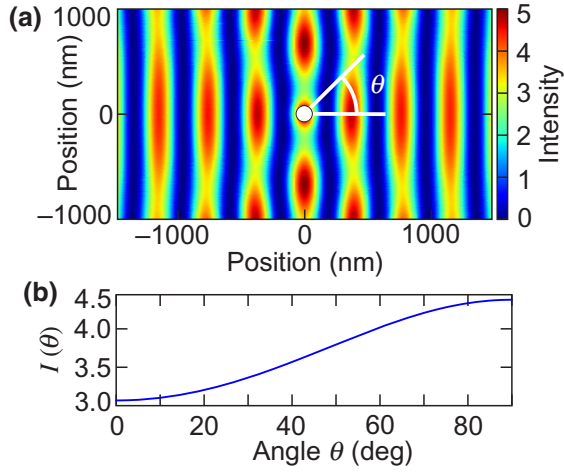


FIG. 6. (a) The optical intensity around a nanofiber (white circle,  $d = 150$  nm), which is located at the position of the antinode of a  $p$ -polarized standing wave. The intensity is normalized to that of a single incoming plane wave, i.e., without the nanofiber, we have  $I = 4$  in the antinodes of the standing wave. The local intensity at the nanofiber surface exceeds this value at certain positions around the fiber. This is also apparent in (b), where this local intensity is plotted against the azimuthal angle.

exist. In this case, the presence of the fiber influences which mode is excited. To illustrate this connection, we excite the  $TEM_{10}$  mode, which has a node line in the  $x$  direction. Due to the cylindrical geometry of the cavity, the  $TEM_{10}$  mode is near degenerate with the  $TEM_{01}$  mode, which has a node line in the  $y$  direction. As the fiber with its axis parallel to the  $y$  direction is moved into the mode, the observed finesse first goes down, similar to the situation with the  $TEM_{00}$  mode (see Fig. 5). However, in the very center of the mode the finesse increases again to a value comparable to the case without fiber. At the same time, the transverse intensity profile in the cavity turns around the cavity axis by  $90^\circ$  where the fiber axis coincides with the node line of the  $TEM_{01}$  mode. This observation can be understood as caused by a mode-dependent interaction: without nanofiber, both modes are excited depending on their geometric overlap with the incoming laser beam. In the situation of Fig. 5 the incoming laser beam is adjusted to mainly excite the  $TEM_{10}$  mode; however, also the  $TEM_{01}$  mode is slightly excited (not visible in the image). As the nanofiber is introduced into the cavity the modes suffer both losses and a dispersive phase shift depending on the overlap of the respective mode intensity with the nanofiber. In the very center of the cavity where the overlap with the  $TEM_{10}$  mode and  $TEM_{01}$  mode is maximum and minimum, respectively, the different dispersive phase shifts lift the degeneracy of the two modes. Thus, the  $TEM_{01}$  mode can be separately excited without loss for a certain laser frequency, whereas the  $TEM_{10}$  mode, which suffers loss, is shifted to a different

frequency. The data shown in Fig. 5 are obtained with the  $d = 1\text{-}\mu\text{m}$ -diameter fiber where this effect is strongest. We observe that the mode rotation gets weaker for decreasing fiber diameter, consistent with a smaller dispersive shift of the  $TEM_{10}$  mode. We will investigate the phase shift quantitatively in future work. Figure 5 compares the experimental data with the results from our model. The red lines correspond to a loss rate as expected for the  $TEM_{00}$  mode with no node line in the center, and the black lines correspond to a loss rate as expected for the  $TEM_{01}$  mode with intensity profile

$$I(x, y) = I_0 e^{-2 \frac{x^2 + y^2}{w_0^2}} \left( \frac{\sqrt{2}x}{w_0} \right)^2. \quad (17)$$

#### IV. CONCLUSION

This paper analyzes the optical losses in a cavity caused by light scattering from an optical nanofiber, and its dependence on the fiber diameter and polarization of the mode. For the smallest fiber diameter tested ( $d = 150$  nm) the round-trip loss is of the order of  $L = 0.001$  such that the cavity finesse with fiber in the center of the mode reaches a value of the order of  $F = 1000$ . Thus, the fiber might be a very useful substrate to investigate the optical properties of single nanoparticles in high-finesse cavities. The fiber-induced loss could be reduced even further by positioning the fiber in a node of the standing wave in the cavity, if the fiber axis is aligned perpendicular to the cavity axis. But also the coupling to an emitter will depend on the position in the standing wave. This is illustrated in Fig. 6, where we calculate the optical intensity around a nanofiber in a  $p$ -polarized standing wave. Compared with the standing wave alone, the local intensity at the fiber surface and, thus, the atom-light coupling strength can be enhanced. We also show that, despite the concomitant decrease in finesse, decreasing the beam waist is favorable for reaching strong light-matter interactions. Our future setup will take this dependency into account by minimizing the radius of the cavity mode. An interesting feature is also observed for the degenerate  $TEM_{10}$  and  $TEM_{01}$  modes where the position of the fiber determines which mode is excited. An even richer behavior can be expected for confocal or concentric cavities that facilitate many degenerate modes. Another interesting perspective is the possibility of coupling the cavity modes to light propagating along the fiber as an evanescent wave. A nanoparticle attached to the fiber could serve as a switchable interface between the fiber and cavity mode with applications in sensing and single-photon generation. Another perspective of the setup is the investigation of quantum Mie scattering [26].

- [1] D. S. Dovzhenko, S. V. Ryabchuk, Y. P. Rakovich, and I. R. Nabiev, Light-matter interactions in the strong coupling regime: Configurations, conditions, and applications, *Nanoscale* **10**, 3589 (2018).
- [2] T. Yoshie, A. Scherer, J. Hendrickson, G. Khitrova, H. M. Gibbs, G. Rupper, C. Ell, O. B. Shchekin, and D. G. Deppe, Vacuum rabi splitting with a single quantum dot in a photonic crystal nanocavity, *Nature* **432**, 200 (2004).
- [3] D. Englund, B. Shields, K. Rivoire, F. Hatami, J. Vučković, H. Park, and M. D. Lukin, Deterministic coupling of a single nitrogen vacancy center to a photonic crystal cavity, *Nano Lett.* **10**, 3922 (2010).
- [4] J. P. Reithmaier, G. Sek, A. Löffler, C. Hofmann, S. Kuhn, S. Reitzenstein, L. V. Keldysh, V. D. Kulakovskii, T. L. Reinecke, and A. Forchel, Strong coupling in a single quantum dot–semiconductor microcavity system, *Nature* **432**, 197 (2004).
- [5] E. Peter, P. Senellart, D. Martrou, A. Lemaitre, J. Hours, J. M. Gerard, and J. Bloch, Exciton-Photon Strong-Coupling Regime for a Single Quantum dot Embedded in a Microcavity, *Phys. Rev. Lett.* **95**, 067401 (2005).
- [6] P. E. Barclaya, K.-M. C. Fu, C. Santori, and R. G. Beausoleil, Chip-based microcavities coupled to nitrogen-vacancy centers in single crystal diamond, *Appl. Phys. Lett.* **95**, 191115 (2009).
- [7] Y. Sugawara, T. A. Kelf, J. J. Baumberg, M. E. Abdelsalam, and P. N. Bartlett, Strong Coupling between Localized Plasmons and Organic Excitons in Metal Nanovoids, *Phys. Rev. Lett.* **97**, 266808 (2006).
- [8] G. Zengin, M. Wersall, S. Nilsson, T. J. Antosiewicz, M. Kall, and T. Shegai, Realizing Strong Light-Matter Interactions between Single-Nanoparticle Plasmons and Molecular Excitons at Ambient Conditions, *Phys. Rev. Lett.* **114**, 157401 (2015).
- [9] R. Chikkaraddy, B. de Nijs, F. Benz, S. J. Barrow, O. A. Scherman, E. Rosta, A. Demetriadou, P. Fox, O. Hess, and J. J. Baumberg, Single-molecule strong coupling at room temperature in plasmonic nanocavities, *Nature* **535**, 127 (2016).
- [10] J. Ye, D. W. Vernooy, and H. J. Kimble, Trapping of Single Atoms in Cavity qed, *Phys. Rev. Lett.* **83**, 4987 (1999).
- [11] A. Chizhik, F. Schleifenbaum, R. Gutbrod, A. Chizhik, D. Khoptyar, A. J. Meixner, and J. Enderlein, Tuning the Fluorescence Emission Spectra of a Single Molecule with a Variable Optical Subwavelength Metal Microcavity, *Phys. Rev. Lett.* **102**, 073002 (2009).
- [12] M. Mader, J. Reichel, T. W. Hänsch, and D. Hunger, A scanning cavity microscope, *Nat. Commun.* **6**, 7249 (2015).
- [13] T. Delord, P. Huillery, L. Nicolas, and G. Hétet, Spin-cooling of the motion of a trapped diamond, *Nature* **580**, 56 (2020).
- [14] L. Dania, D. S. Bykov, M. Knoll, P. Mestres, and T. E. Northup, Optical and electrical feedback cooling of a silica nanoparticle levitated in a paul trap, *Phys. Rev. Res.* **3**, 013018 (2021).
- [15] U. Delic, M. Reisenbauer, K. Dare, D. Grass, V. Vuletić, N. Kiesel, and M. Aspelmeyer, Cooling of a levitated nanoparticle to the motional quantum ground state, *Science* **367**, 892 (2020).
- [16] F. Warken, A. Rauschenbeutel, and T. Bartholomaus, Fiber pulling profits from precise positioning - precise motion control improves manufacturing of fiber optical resonators, *Photonics Spectra* **3**, 73 (2008).
- [17] M. Fujiwara, K. Toubaru, T. Noda, H.-Q. Zhao, and S. Takeuchi, Highly efficient coupling of photons from nanoemitters into single-mode optical fibers, *Nano Lett.* **1**, 4362 (2011).
- [18] R. Yalla, F. LeKien, M. Morinaga, and K. Hakuta, Efficient Channeling of Fluorescence Photons from Single Quantum Dots Into Guided Modes of Optical Nanofiber, *Phys. Rev. Lett.* **109**, 063602 (2012).
- [19] S. M. Skoff, D. Papencordt, H. Schauffert, B. C. Bayer, and A. Rauschenbeutel, Optical-nanofiber-based interface for single molecules, *Phys. Rev. A* **97**, 043839 (2018).
- [20] Y. Yonezu, K. Wakui, K. Furusawa, M. Takeoka, K. Semba, and T. Aoki, Efficient single-photon coupling from a nitrogen-vacancy center embedded in a diamond nanowire utilizing an optical nanofiber, *Sci. Rep.* **7**, 12985 (2017).
- [21] C. Ding, M. Joos, C. Bach, T. Bienaimé, E. Giacobino, E. Wu, A. Bramati, and Q. Glorieux, Nanofiber based displacement sensor, *Appl. Phys. B* **126**, 103 (2020).
- [22] F. Fogliano, B. Besga, A. Reigue, P. Heringlake, L. MercierdeLepinay, C. Vaneph, J. Reichel, B. Pigeau, and O. Arcizet, Mapping the Cavity Optomechanical Interaction with Subwavelength-Sized Ultrasensitive Nanomechanical Force Sensors, *Phys. Rev. X* **11**, 021009 (2021).
- [23] R. W. P. Drever, J. L. Hall, F. V. Kowalski, J. Hough, G. M. Ford, A. J. Munley, and H. Ward, Laser phase and frequency stabilization using an optical resonator, *Appl. Phys. B* **31**, 97 (1983).
- [24] F. Warken, *Ultradünne Glasfasern als Werkzeug zur Kopplung von Licht und Materie*, Ph.D. thesis, school University of Bonn, Germany (2007), <https://hdl.handle.net/20.500.11811/3141>.
- [25] H. van de Hulst, Light scattering by small particles (Dover publication, New York, 1981) Chap. 15, pp. 297–304, 1st ed.
- [26] P. Maurer, C. Gonzalez-Ballester, and O. Romero-Isart, Quantum electrodynamics with a nonmoving dielectric sphere: Quantizing lorenz-mie scattering, *ArXiv:2106.07975v2* (2021).